Structural Chemistry (2021) 32:135–148
https://doi.org/10.1007/s11224-020-01627-4

ORIGINAL RESEARCH

A molecular docking simulation study on potent inhibitors against *Rhizoctonia solani* and *Magnaporthe oryzae* in rice: silver-tetrylene and bis-silver-tetrylene complexes vs. validamycin and tricyclazole pesticides

Bui Thi Phuong Thuy[1] · Tran Thi Ai My[2] · Nguyen Thi Thanh Hai[2] · Huynh Thi Phuong Loan[2] · Le Trung Hieu[2] · Tran Thai Hoa[2] · Thanh Q. Bui[2] · Ho Nhat Tuong[2] · Nguyen Thi Thu Thuy[3] · Doan Kim Dung[4] · Pham Van Tat[5] · Phan Tu Quy[6] · Nguyen Thi Ai Nhung[2]

Received: 26 May 2020 / Accepted: 24 August 2020 / Published online: 29 August 2020

Abstract

Rice, well known as the most important staple food source worldwide, is highly susceptible to many infectious diseases, especially rice sheath blight caused by fungus *Rhizoctonia solani* and rice blast caused by fungus *Magnaporthe oryzae*. The inhibitory ability of silver- and bis-silver-tetrylene complexes, including **Ag-E** and **bis-Ag-E** with **E** = C, Si, Ge, onto protein 4G9M in *Rhizoctonia solani* and protein 6JBR in *Magnaporthe oryzae* was theoretically investigated using molecular docking simulation methodology. Two commercial pesticides selected as inhibitory references are validamycin for 4G9M and tricyclazole for 6JBR. The results reveal that bis-silver-tetrylene complexes perform the strongest inhibitory effects towards both proteins. The structures of the complexes exhibit good site–site binding to both proteins given the observations on the hydrogen bond interactions, cation–π bonds, π–π bonds, and ionic interactions, interaction distance between amino acids and ligands, and van der Waals interactions. The inhibitory capacity onto protein 4G9M decreases in the following order: **bis-Ag-C** > **bis-Ag-Si** > **bis-Ag-Ge** > validamycin > **Ag-C** ≈ **Ag-Si** ≈ **Ag-Ge**. The corresponding order observed from the study for protein 6JBR is **bis-Ag-C** > **bis-Ag-Si** ≈ **bis-Ag-Ge** > tricyclazole ≈ **Ag-C** ≈ **Ag-Si** ≈ **Ag-Ge**. The study opens a promising approach to tackle rice blast and rice sheath blight based on a family of silver-tetrylene organometallic chemicals given the theoretical proof of environment-advanced properties and molecule-scaled effectiveness.

Keywords Tetrylenes · *Rhizoctonia solani* · 4G9M · *Magnaporthe oryzae* · 6JBR · docking simulation

✉ Nguyen Thi Thanh Hai
nguyenthanhhai@hueuni.edu.vn

✉ Nguyen Thi Ai Nhung
ntanhung@hueuni.edu.vn

[1] Faculty of Basic Sciences, Van Lang University, Ho Chi Minh City 700000, Vietnam

[2] Department of Chemistry, University of Sciences, Hue University, Hue 530000, Vietnam

[3] Faculty of Agronomy, University of Agriculture and Forestry, Hue University, Hue 530000, Vietnam

[4] Research Institute for Biomedical Science, Tokyo University of Science, 2669 Yamazaki, Noda, Chiba 278-0022, Japan

[5] Institute of Development and Applied Economics, Hoa Sen University, Ho Chi Minh City 700000, Vietnam

[6] Department of Natural Sciences & Technology, Tay Nguyen University, Buon Ma Thuot 630000, Vietnam

Introduction

Rice (*Oryza sativa* L.) is rich in nutrients, vitamins, and minerals, and by far the most important staple food source for more than 70% of the world's population [1]. The demand for rice production has seen a dramatic increase in recent years due to the rapid growth of the global population. However, rice is vulnerable to many diseases caused by microorganisms such as bacteria, viruses, or fungi, leading to dramatic losses in the crop yield annually. Rice blast and rice sheath blight, caused by fungi *Magnaporthe oryzae* and *Rhizoctonia solani* respectively, are two of the most devastating diseases and result in severe impacts on either rice yield or grain quality.

Sheath blight results in yield loss of 10–25% [2] and up to 50% under favorable environmental conditions [3]. Sheath blight is recognizable by the rapid and irregular appearance

of light gray to dark brown lesions before they coalesce to cover across larger portions of the sheath and leaf lamina. It is caused by *Rhizoctonia solani* (*R. solani*), a soil-borne fungus. Although there are many groups of *R. solani* species, the most populated *R. solani* transcripting in glutenin is known as *R. solani agglutinin*. Figure 1a shows the structure of 4G9M, a lectin-type protein accumulated in the mycelium and sclerotia of *R. solani* and serving as a storage protein. It also involves in the morphogenesis and development of the fungi.

Meanwhile, *Magnaporthe oryzae* (*M. oryzae*) attacks all parts of rice plant, including leaves, leaf collars, necks, panicles, pedicels, and seeds. This can happen at any stage of the plant growth and often results in yield loss as high as 30% [4]. *M. oryzae*, a heterothallic fungus, infects the plant by its conidia via appressoria. This cellular type accumulates a high concentration of glycerol and forms a dense layer of melanin. The accumulation of the melanin is an essential step before the appressoria of *M. oryzae* penetrate into host plants. The synthesis of melanin is aggressively catalyzed by glycosyltransferase superfamily, especially an enzyme named 6JBR. It accounts for the transfer of glycosyl groups from an activated nucleotide sugar to a nucleophilic glycosyl acceptor. Figure 1b illustrates the structure of *M. oryzae* protein 6JBR. Subsequently, the fungus elaborates the invasion to the underlying plant cells in a very short time. The molecules inhibiting *M. oryzae* induces melanin-deficient mutants, resulting in the fungus losing its capacity to infect the host plants. Melanin biosynthesis inhibitors can play the role as a reductase, such as tricyclazole and pyroquilon. Tricyclazole is a systemic fungicide, causing a great reduction in glycerol accumulation in *M. oryzae* appressoria and inhibiting enzymes 6JBR in the biosynthetic pathway of melanin. Thus, *M. oryzae* undergoes the deficiency of pathogen penetrability into the host.

Validamycin (Fig. 2a) is an antibiotic widely used to fight *R. solani*. Validamycin alters the morphology of *R. solani* by inhibiting the glucose conversion to lectin as transported into the plant cell and hydrolyzed therein, consequently preventing the spread of the fungus. Although synthetic fungicides are often recommended for prohibiting plant pathogens in agriculture, the drawback is that their residues leave serious, long-lasting effects on environment and human health. Moreover, fungi are highly variable, and it there is an emergence of potential risks such as fungicide resistant germs [4] or eliminating beneficial insects [5] with high-dose or multiple use of fungicides. Likewise, in Vietnam, Beam 75WP and validamycin 5L, containing active materials tricyclazole and validamycin, are commonly utilized to control rice blast and rice sheath blight, respectively. The concerns of negative consequences by over-dosing or long-term uses are also apparent. The shortcoming in finding safety inhibitors has driven for the regulation in plant disease management to minimize the toxicity of chemicals. Silver ions or silver nanoparticles possess distinct antimicrobial activity and have been widely used for many sterilization purposes. Many evidences have been reported about cytotoxicity of silver nanoparticles to fungi. For example, silver nanoparticles stabilized in hyperbranched polymers (size 1.4 to 7.1 nm) and stabilized with Myramistin (size 10 nm) inhibited the growth of *A. niger* and *S. cerevisiae* [6–8]. Furthermore, 3-nm silver nanoparticles were found toxic towards *T. mentagrophytes* and *C. albicans* [9–11].

In current usage, tricyclazole (Fig. 2b) is widely used to treat *M. oryzae* causing blast rice disease. Tricyclazole (5-methyl-1,2,4-triazolo[3,4-b]benzothiazole) has been known since the 1980s as a treatment of rice blast, in seed as well as systemic fungicide [12–14]. Tricyclazole is a fertilizer strongly absorbable through roots and leaves of rice plants. The compound inhibits the formation of melanin in the germ

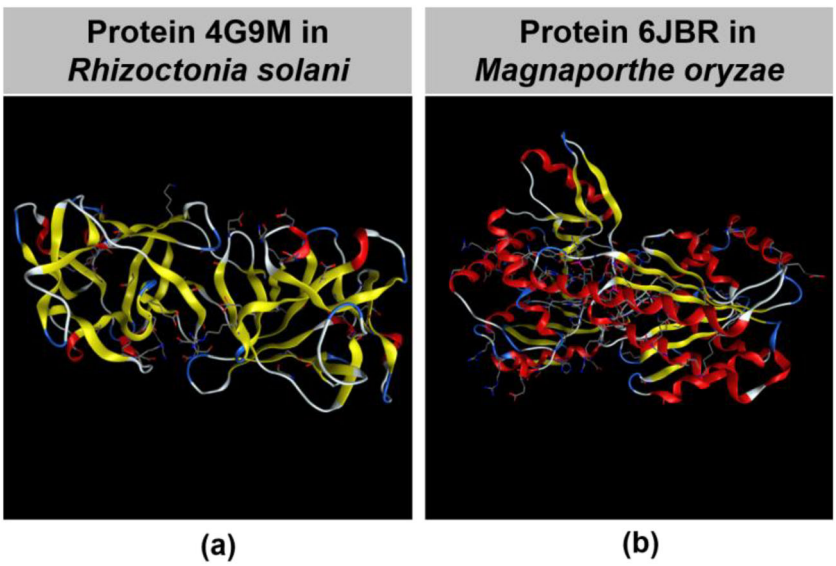

Fig. 1 **a** Protein 4G9M (DOI: https://doi.org/10.2210/pdb4G9M/pdb) in *Rhizoctonia solani* and **b** protein 6JBR in *Magnaporthe oryzae* (DOI: https://doi.org/10.2210/pdb6JBR/pdb), referenced from Worldwide Protein Data Bank

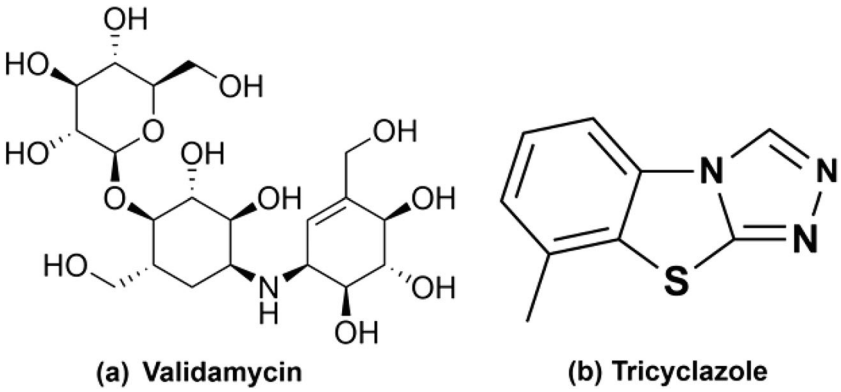

Fig. 2 The widely used pesticides. **a** Validamycin. **b** Tricyclazole

cell of hyphae. As a result, the fungi are impeded to penetrate the leaf cell tissue of the host plant. Tricyclazole is commonly used to eradicate blast disease (*M. oryzae*) in both transplanted rice and direct sowing. Recently, it is still used to treat *M. oryzae* in rice [15, 16] although the European Commission had reduced maximum residues level for tricyclazole to 0.01 mg kg^{-1} for all crops since 30 December 2017 [17]. Besides, validamycin has long been used in Vietnam, China, India, etc. to deal with sheath blight in rice, corns, and other crops [18, 19] thanks to its capacity to inhibit trehalase, interfering the fungal energy metabolism. The pesticide has been widely used to prevent the growth of *R. solani* but cannot degrade it [20, 21]. The reason could be due to the resistance of the pathogen to the chemical fungicide [21].

In recent years, there have been a number of researches embarking on the application of silver products to tackle the plant diseases. A report revealed the effectiveness of silver nanoparticles on controlling *Colletotrichum* species in vitro and pepper anthracnose disease on the field [22]. Other studies also showed that biosynthesized silver nanoparticles are deemed as "a nano-weapon" against phytopathogens and they have potential applications in agriculture [23]. Although the mechanisms of the biological activity of silver in either ionic or nanoparticle form on bacteria and fungi are still not entirely clear, some toxicity-based mechanisms are proposed. According to a report, silver accumulates on bacterial membrane causing certain modification of permeability, which eventually leads to the subsequent release of lipopolysaccharides, proteins, and intracellular biomolecules and the dissipation of the proton-motive force across the plasma membrane [24]. Another theory suggests that the cell structure of bacteria could be deteriorated by the oxidation of active oxygen species (ROS) which are produced by ions released from silver nanoparticles [25]. Also, the absorption of metallic ions derived from the surface of nanomaterials can reduce intracellular ATP formation and disrupt DNA replication [26]. In addition, silver ions released from the nanoparticle surface may interact with biomolecules containing phosphorus and sulfur such as DNA and proteins, thus deforming their structures and breaking their biochemical processes up [27].

Versatile ligands N-heterocyclic carbenes (NHCs) are widely used from homogeneous catalysis to material science in coordinative and organometallic chemistry. NHC ligands belong to the tetrylene ligand family NHE, where **E** = C (carbene), Si (silylene), Ge (germylene), etc., which are stable and able to coordinate to various metallic centers making them highly applicable in various chemical fields [28]. An N-heterocyclic carbene ligand comprises a free singlet lone pair electron, and the other pair electrons bind to R (C – R) which is a neutral donor ligand rich of electrons. Therefore, investigation on applications of the NHC-metal complexes has attracted great attention. The carbodicarbenes $C(NHC)_2$ were synthesized and structurally analyzed by Bertrand et al. [29], and a parallel study was also reported by Fürstner's team [30]. Recently, silver complexes derivative NHCs have been extensively investigated for monitoring against different plant pathogenic fungi [31]. In addition, they have been investigated to develop potential antibacterial and anti-cancer agents possessing low inhibiting concentrations [31, 32]. Also, NHCs can act as intermediate agents for various organic metabolic reactions thanks to the primary attachment of NHC ligands to carbonyl groups. Besides, the ester metabolism reaction using aldehyde as a substrate is mainly catalyzed by NHCs [33].

In this study, the inhibitory ability of silver- and bis-silver-tetrylene complexes, including **Ag-E** and **bis-Ag-E** with **E** = C, Si, Ge, on protein 4G9M [34] of fungi *R. solani* and protein 6JBR [35] of fungi *M. oryzae* is theoretically investigated. The structures of NHCs and its homologous compounds combining silver chloride complexes are illustrated in Fig. 3. The information on site–site binding interactions between the complexes and the proteins is obtained using molecular docking simulation methodologies. The results are presented through configurations of the ligands; the docking score energy (DS); root-mean-square deviation (RMSD); types of interactions such as hydrogen bonds, cation–π, π–π bonds, and ionic interactions, interaction distance between amino acids, site–site binding, and van der Waals interactions; and respective distances between the ligands and proteins. The results of this study could contribute as a database to open up other

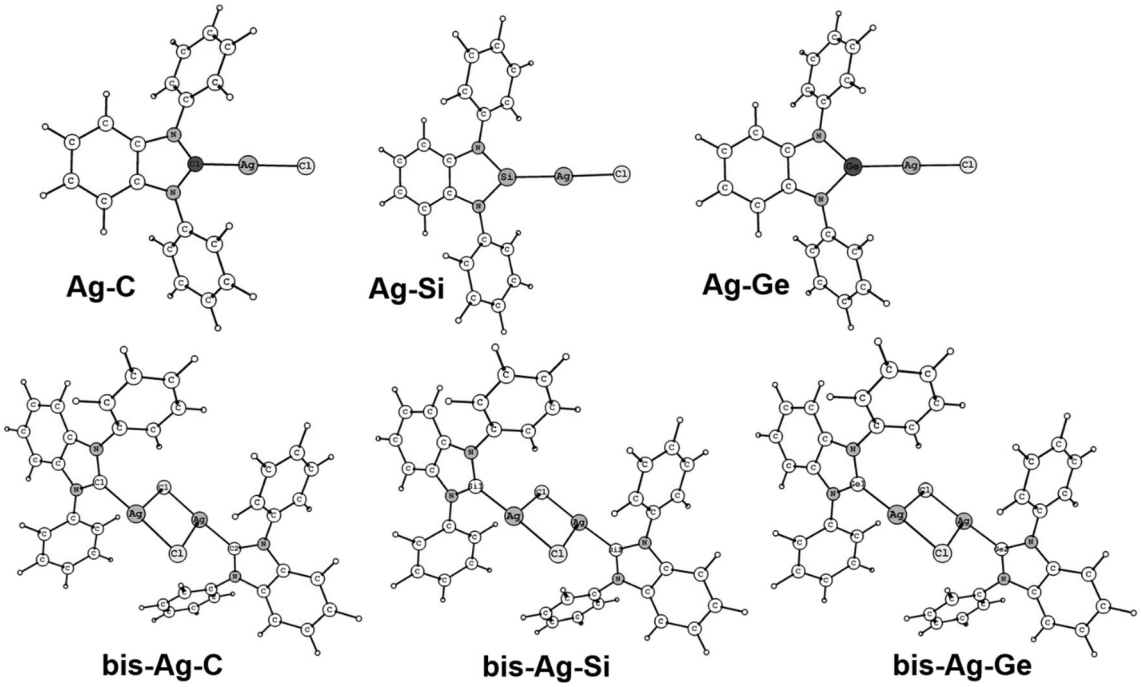

Fig. 3 Structures of the studied complexes in this study: silver-tetrylenes **Ag-E** and bis-silver-tetrylenes **bis-Ag-E** (**E** = C, Si, Ge)

research directions on the flexibility of silver-tetrylene and bis-silver-tetrylene complexes applied in plant protection in general and agriculture in particular. Besides, the simulation is carried out on the two widely used pesticides, i.e., validamycin and tricyclazole, as references. To the best of our knowledge, there has been neither experimental nor theoretical research reported on using silver-tetrylene and bis-silver-tetrylene complexes for the inhibition of *R. solani* causing sheath blight of rice and *M. oryzae* causing blast rice disease. The investigated complexes in this study can be considered as new families of plant protection products.

Molecular docking simulation methodology

Protein and ligand preparation

Crystal structures of protein 4G9M in *R. solani* and protein 6JBR in *M. oryzae* were obtained from Worldwide Protein Data Bank [35]. The molecular data of silver-tetrylene complexes and the commercial pesticides was referenced from the literature [36]. The silver-tetrylene complexes are denoted as **Ag-C**, **Ag-Si**, **Ag-Ge**, **bis-Ag-C**, **bis-Ag-Si**, and **bis-Ag-Ge** (Fig. 3). Validamycin and tricyclazole are selected as the referenced pesticides (Fig. 2). The Sequence Editor of the program Molecular Operating Environment (MOE) 2015.10 [37] was used to plot chemical structures of the compounds. The ligands were energy-optimized via Conj Grad and Termination. The optimization parameters were set as follows: energy change 0.0001 kcal mol^{-1}; maximum interactions 1000; and modified charge Gasteiger–Huckel. Afterwards, the energy minimization of all molecules was carried out. Quickprep tool was used to prepare the protein structures and their 3D protonation, whose configurations include Tether – Receptor with the strength of 5000; and Refine of 0.0001 kcal $mol^{-1}·Å^{-1}$. Active zones of the proteins were determined based on the ligand position within a radius of 4.5 Å and the presence of important amino acids. The information of protein structures was saved in *.pdb format. Finally, molecular interactions were carried out on the system MOE 2015.10, and the achieved molecule structures were saved in *.sdf format.

Protein structure validation

Before performing molecular docking simulation, the crystal structures of protein 4G9M in *R. solani* and protein 6JBR in *P. oryzae* were cross-checked to confirm the positions of their amino acids in the active sites. The active site and the binding active site of 4G9M and 6JBR were found comprising essential amino acids Asn 129, Leu 108, Gly 43, Arg 289, and Asp 153 [34, 38].

Molecules docking into proteins: docking investigation

Molecular docking simulation between the complexes and the proteins was investigated using MOE 2015.10 software. The parameters were prepared by calculating the number of poses to keep for further analysis of interaction. These

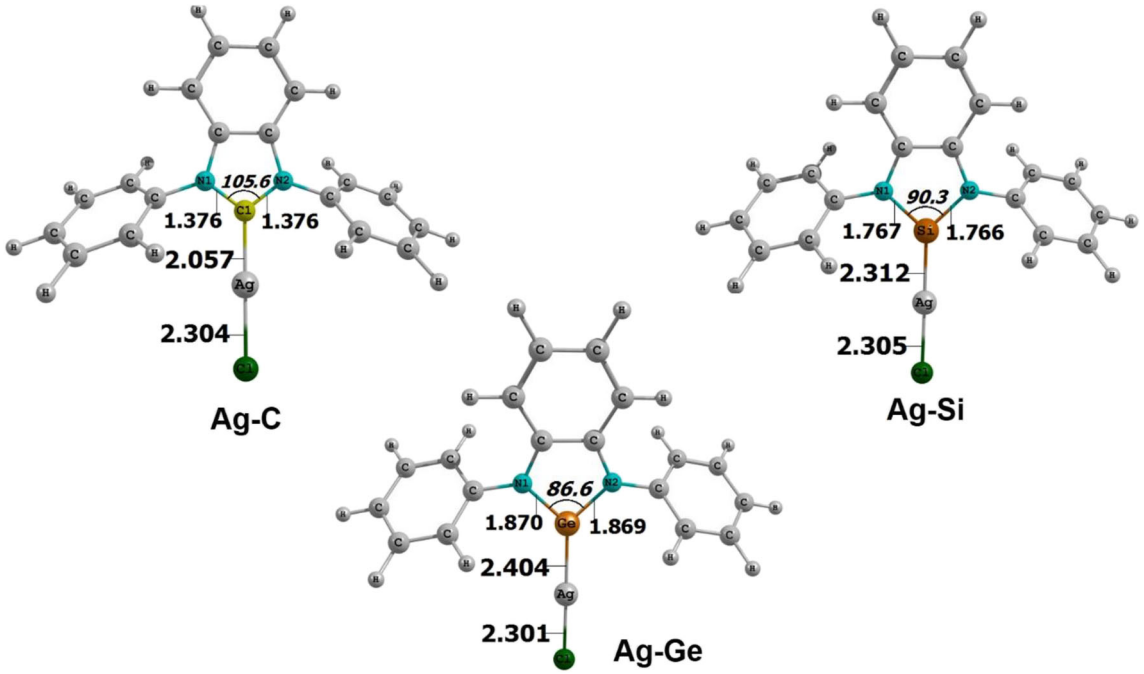

Fig. 4 Optimized structures of silver-tetrylene complexes **Ag-E** (**E** = C, Si, Ge) using BP86/def2-SVP computations. Bond lengths are given in Å and angles in degrees

configurations were set at 10. The maximum number of solutions per iteration was 1000. The maximum number of solutions per fragmentation was 200.

Molecular docking studies analysis

Docking score energy (DS) and root-mean-square deviation (RMSD) provide the interaction information of the ligands and the proteins. The root-mean-square deviation cluster was set up to 2.0 Å in each run. The analysis of the interactions formed between ligands and important amino acids in the site–site distances was implemented. Hydrogen bonds, ion bonds, arene–arene (π–π), cation–arene (cation–π), and van der Waals interactions were detected. The evaluation of DS explains the analysis of the interaction between the compounds and the targeted proteins. The interactions are

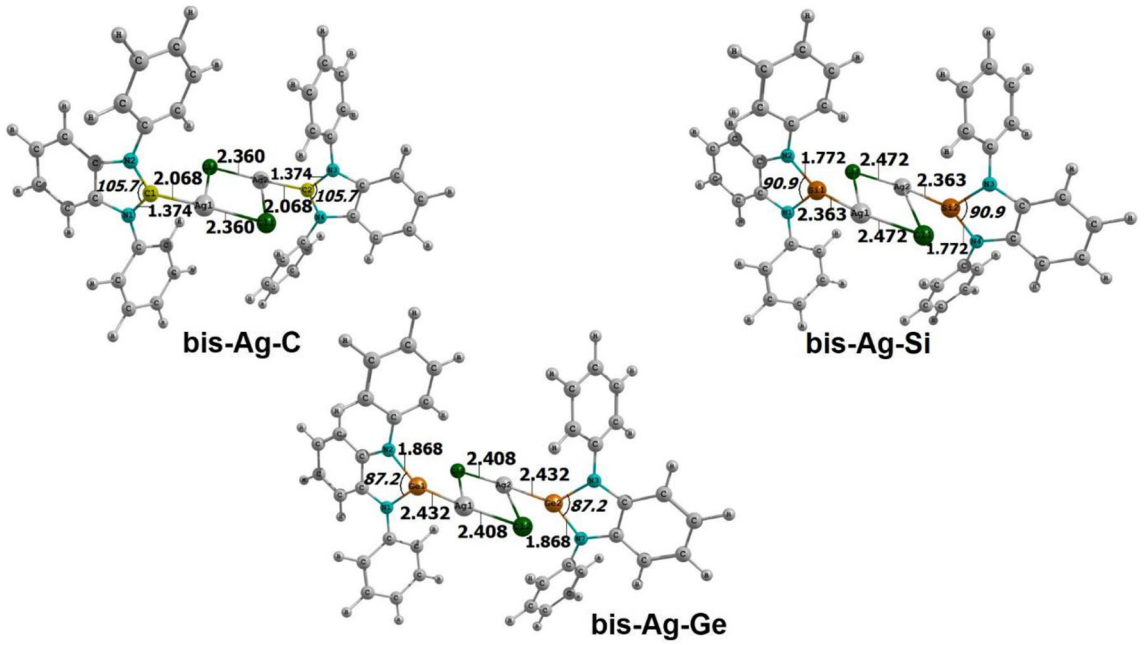

Fig. 5 Optimized structures of bis-silver-tetrylene complexes **bis-Ag-E** (**E** = C, Si, Ge) using BP86/def2-SVP computations. Bond lengths are given in Å and angles in degrees

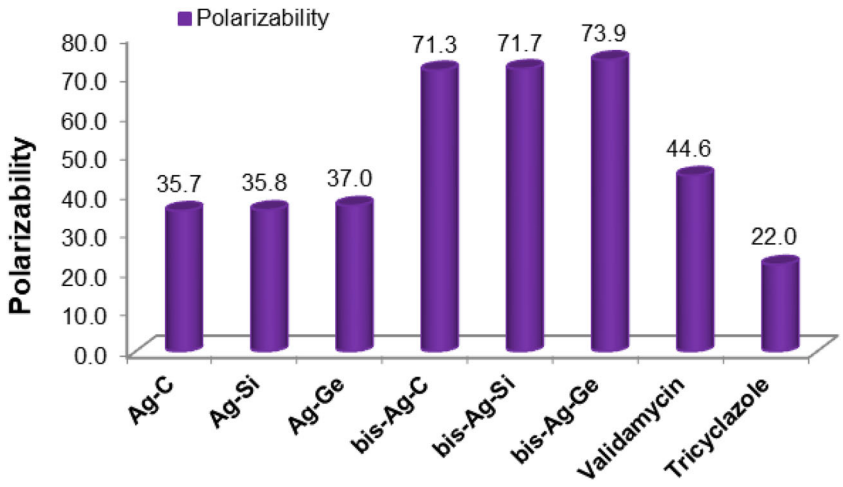

Fig. 6 Polarizability values (Å^3) of silver-tetrylene complexes **Ag-E** and bis-silver-tetrylene complexes **bis-Ag-E** (**E** = C, Si, Ge) compared with the validamycin and tricyclazole fungi

displayed on 2D and 3D planes. Various interactions such as van der Waals interactions, hydrogen bonds, cation–π, π–π bonds, ionic interactions, and interaction distance between amino acids and the active sites of compounds were plotted. van der Waals interactions were detected by contact between hydrophilic and hydrophobic surfaces, the substances and the bonding point and the ligand–protein interactions determined.

Results and discussion

Geometrical structures of silver-tetrylene complexes **Ag-E** and bis-silver-tetrylene complexes **bis-Ag-E** (**E** = C, Si, Ge) are optimized using density functional theory with the BP86 functional and the def2-SVP basis set with the aid of Gaussian09 program [39]. Optimized structures and parameters of complexes **Ag-E** and **bis-Ag-E** are presented in Figs. 4 and 5, respectively. Complex **Ag-C** contains silver-carbene with bond length of 2.057 Å, accounting for the shortest value observable. The corresponding figure increases from silver-carbene to silver-germylene and registers its highest value at 2.404 Å in complex **Ag-Ge**. This is consistent with the tendency of **Ag-E** (**E** = C, Si, Ge) bond lengths (2.076–2.448 Å) in the less bulky silver-tetrylene complexes AgCl-NHE_H calculated by Frenking et al. [38]. The bis-(**Ag-C**) bond lengths in the **bis-Ag-C** exhibit the same values as 2.068 Å (Fig. 5). They are rather similar to the bis-(Ag-C) bond lengths Ag1-C and Ag2-C (2.084 Å) in silver-carbodicarbene [$(NHC_H)_2$-Ag] calculated in another report [38]. The optimized structures of the heavier homologues, **bis-Ag-Si** and **bis-Ag-Ge**, are displayed the elaborate **bis-(Ag-Si)** and **bis-(Ag-Ge)** bond lengths as 2.363 and 2.432 Å in comparison with those in the **bis-Ag-C** adduct.

Stable structures of silver-tetrylene (**Ag-C** – **Ag-Ge**) and bis-silver-tetrylene (**bis-Ag-C** – **bis-Ag-Ge**) complexes are evaluated by computing polarizability (Å^3) implemented on QSARIS system with the Gasteiger–Marsili method [40]. The obtained parameters are presented in Fig. 6. The polarizability

Table 1 Docking simulation results: docking score energy (DS), root-mean-square deviation (RMSD) and interactions with 4G9M amino acids of silver-tetrylene, bis-silver complexes (**Ag-E** and **bis-Ag-E** with **E** = C, Si, Ge), and validamycin

Complex	Symbol (complex-protein)	DS (kcal·mol^{-1})	RMSD (Å)	Interaction with amino acid
Ag-C	**[Ag-C]-4G9M**	− 9.6	0.80	Asp A105, Arg A107, Glu B102, Asp A91, Gly A55, Arg B107, Lys B54, Asn A56, Asn B128, Asn B130, Gln A57
Ag-Si	**[Ag-Si]-4G9M**	− 11.9	1.19	Asn B129, Gln A57, Gly A55, Lys A54, Asn A 56, Arg A107, Arg B107, Asp A91.
Ag-Ge	**[Ag-Ge]-4G9M**	− 10.2	1.30	Leu B108, Glya55, Asn B130, Asn A56, Gln A57, Arg B107, Arg A107, Glu B102, Asp A91
bis-Ag-C	**[bis-Ag-C]-4G9M**	− 13.7	1.14	Asn A56, Glu B102, Ala A104, Asp A105, Thr B132, Leu B108, Gln A57, His A106, Gly A53, Arg B107
bis-Ag-Si	**[bis-Ag-Si]-4G9M**	− 12.7	1.93	Asp A105, Arg A107, Glu B102, Asp A91, Thr B132, Ala B131, Asn A56, Gln A57, Gly A53
bis-Ag-Ge	**[bis-Ag-Ge]-4G9M**	− 12.5	1.24	Tyr B127, Gln A57, Asp A105, Lys A54, Arg A107, Asn A56, Gly A55, Glu B102, Asp A91, Thr B132
Validamycin	Validamycin-4G9M	− 12.3	1.06	Gly B55, Gln B57, Ala B104, His B106, Arg A107, Leu A108, Asn A129, Asn A130

Table 2 Molecular docking simulation results with critical interactions between the complexes and 4G9M amino acids: interaction distance between amino acids, site–site binding, energy, cation–π, π–π bonds, ionic interactions, and total hydrogen bonds

Complex (ligand–protein)	Ligand	Protein		Interactions	Distance (Å)	Energy (kcal·mol^{-1})	Hydrogen bonds
Ag-C-4G9M	Cl	O	Leu 108	H–donor	3.04	− 1.2	2
	Ag	O	Asn 129	Metal	2.76	− 1.3	
Ag-Si-4G9M	Cl	O	Glu 102	H–donor	3.69	− 0.5	3
	Si	C	Leu 108	H–acceptor	3.98	− 0.9	
	Ag	O	Glu 102	Metal	2.61	− 1.3	
Ag-Ge-4G9M	Ge	N	Asn 128	H–acceptor	4.31	− 1.2	2
	Ag	O	Asn 129	Metal	2.93	− 0.5	
bis-Ag-C-4G9M	Cl	N	Asn 128	H–acceptor	3.45	− 4.2	4
	Cl	C	Asn 130	H–acceptor	4.11	− 2.9	
	Cl	C	Lys 54	H–acceptor	3.92	− 1.3	
	Ag	O	Asn 129	Metal	2.66	− 2.0	
bis-Ag-Si-4G9M	Cl	C	Asn 130	H–acceptor	3.79	− 1.5	4
	Cl	N	Gly 55	H–acceptor	3.21	− 11.6	
	Ag	O	Asn 129	Metal	2.72	− 2.6	
	5-ring	C	Lys 54	π–H	3.79	− 1.3	
bis-Ag-Ge-4G9M	Cl	N	Gly 55	H–acceptor	3.24	− 10.2	3
	Cl	C	Asn 130	H–acceptor	3.95	− 0.8	
	Ag	O	Asn 129	Metal	2.66	− 3.1	
Validamycin-4G9M	O	O	Asp 105	H–donor	3.00	− 2.6	6
	O	N	Arg 107	H–acceptor	3.20	− 1.2	
	O	C	Lys 54	H–acceptor	3.77	− 0.6	
	O	C	Lys 54	H–acceptor	3.64	− 0.8	
	O	N	Lys 54	H–acceptor	3.31	− 5.7	
	O	N	Arg 107	H–acceptor	2.89	− 3.2	

values of silver-tetrylenes **Ag-E** are in a marginal differential between 35. 7 and 37.0 Å^3. This means they are all lower than the corresponding value of validamycin (44.6 Å^3). However, the polarizability value of tricyclazole (22.0 Å^3) registers the lowest value among the studied complexes. Notably, the bis-silver-tetrylene complexes **bis-Ag-C**, **bis-Ag-Si**, and **bis-Ag-Ge** exhibit their polarizability values at 71.3 Å^3, 71.7 Å^3, and 73.9 Å^3. These are significantly higher than those of both the complexes **Ag-E** and the two pesticides. The results indicate that **Ag-E** and **bis-Ag-E** complexes selected in this study are significantly polarized, which might be conducive to more pronounced inhibitory effects of the two proteins in comparison with the ones that the two pesticides might perform. It is expected that a large value of polarizability could be an important indicator to evaluate the ability of ligands to inhibit the proteins 4G9M and 6JBR. The reasoning is due to the fact that physiological medium in general and its functioning structures in particular are activated by certain degrees of polarizability. In fact, proteins, one of the basic components of any living system, are made of chains of amino acids. All amino acids are polarized molecules as they contain a basic amino group and an acidic carboxyl group. Therefore, the inhibitability of a ligand towards a physiological protein seems to be more pronounced if it possesses a desirable level of polarizability. Otherwise, there is a significant difference in terms of molecular mass (Da) and volume or size (Å) among silver-tetrylenes, which is much smaller when compared with bis-silver-tetrylenes when each complex is docked with proteins 4G9M and 6JBR. Therefore, molecular mass (Da) and volume or size (Å) of the six studied complexes are not included in this study.

The molecular docking simulation of silver-tetrylenes **Ag-E** and bis-silver-tetrylenes **bis-Ag-E** onto protein 4G9M of *R. solani* and protein 6JBR of *M. oryzae* was investigated by program MOE 2015.10. The results for the investigation on protein 4G9M are presented in Figs. 7 and 8 and Tables 1 and 2, while the corresponding data for protein 6JBR is expressed in Figs. 9 and 10 and Tables 3 and 4. Also, Fig. 11 gives the 2D and 3D illustrations of 4G9M-validamycin and 6JBR-tricyclazole docking simulation.

The inhibitability of the ligands towards protein 4G9M is evaluated via root-mean-square deviation (RMSD) value, docking score (DS) energy, and types of interactions. The root-mean-square deviation values are always smaller than 2 Å in all systems. DS values for **bis-Ag-C**, **bis-Ag-Si**, and **bis-Ag-Ge** are − 13.7 kcal mol^{-1}, − 12.7 kcal mol^{-1}, and − 12.5 kcal mol^{-1}, respectively. Meanwhile, silver-tetrylene complexes **Ag-E** show weaker interactions with DS values

Table 3 Docking simulation results: docking score energy (DS), root-mean-square deviation (RMSD), and interactions with 6JBR amino acids of silver-tetrylene, bis-silver complexes (**Ag-E** and **bis-Ag-E** with **E** = C, Si, Ge), and tricyclazole

Complex	Symbol (complex-protein)	DS (kcal·mol^{-1})	RMSD (Å)	Interaction with amino acid
Ag-C	**[Ag-C]-6JBR**	− 12.9	1.52	Leu 392, Asp 388, Asn 391, Ser 41, Tyr 54, Arg 22, Asp 153, Leu 44, Arg 327, His 181, Thr 182, Trp 108, Met 390, Val 393, Lys 294
Ag-Si	**[Ag-Si]- 6JBR**	− 13.4	1.30	Asn 21, Arg 22, His 155, His 181, Ile 251, Met 390, Gly 389, Asp 388, His 212, Lys 294, Gly 43, Arg 289, Ser 41, Arg 327
Ag-Ge	**[Ag-Ge]-6JBR**	− 12.9	1.56	Val 393, Asp 388, Tyr 154, Lys 294, Asn 391, Leu 392, Met 390, Asp 153, Trp 108, Thr 182, His 181, Ser 41, Leu 44, Arg 327, Arg 22, Asp 288
bis-Ag-C	**[bis-Ag-C]-6JBR**	− 16.3	1.69	His 181, Trp 108, Asp 388, Asp 153, Met 390, Asn 391, Val 393, Lys 294, Phe 258, Ser 367, Val 366, Phe 368, Leu 371, Val 287, Leu 44, Ser 41, Arg 22, Arg 327, Val 324, Thr 182
bis-Ag-Si	**[bis-Ag-Si]-6JBR**	− 18.1	1.24	Val 287, Leu 44, Ser 41, Arg 22, Arg 327, Val 394, His 181, Trp 108, Asp 153, Thr 182, Tyr 154, Asp 388, Met 390, Asn 391, Val 393, Lys 294, Phe 258, Ser 367, Val 366, Phe 368, Leu 371
bis-Ag-Ge	**[bis-Ag-Ge]-6JBR**	− 18.4	1.02	Phe 258, Val 393, Met 390, Phe 368, Val 366, Leu 371, Ser 41, Leu 44, Asp 388, Arg 22, Val 287, Lys 294, Tyr 154, Val 324, Asp 288, Asp 153, His 181, Thr 182, Trp 108, Arg 327, Asn 391
Tricyclazole	Tricyclazole-6JBR	− 10.7	1.77	Tyr 154, Tyr 99, His 155, Arg 289, Leu 44, Gly 42, Gly 43, Arg 327, Ser 41

of − 9.6 kcal mol^{-1}, − 11.9 kcal mol^{-1}, and − 10.2 kcal mol^{-1}, respectively for **E** = C, Si, Ge. This could be due to the fact that silver-tetrylene complexes possess relatively smaller volume, lower molecular mass, and polarizability, which lead to low binding capacity with amino acids of the protein. The DS value for validamycin is − 12.3 kcal mol^{-1}, slightly below the corresponding values for bis-silver-tetrylene complexes **bis-Ag-E**. Tables 1 and 2 show that **Ag-C** forms 11 van der Waals interactions and the crucial interactions reside in AgCl of carbene **Ag-C** with –O– of amino acids Leu 108 and Asn 129. Differently, **Ag-Si** creates 8 van der Waals interactions and 3 hydrogen bonds, of which the silicon center atom and AgCl of metal compound mainly interact with –O– and –C– of amino acids Gln 102, Leu 108, and Gln 102. The heavier homologue **Ag-Ge** performs 9 van der Waals interactions and 2 hydrogen bonds with amino acids Asn 128 and Asn 129, and the main interactions lie in Ge and Ag of germylene with –O– and –N– of amino acids. Because **bis-Ag-E** complexes have bulkier tetrylene ligands and metal compounds AgCl than those of **Ag-E** complexes, interactions formed by the bis-carbene are, overall, more than their mono-carbene counterparts. In fact, **bis-Ag-C** adduct creates 10 van der Waals interactions and 4 hydrogen bonds, which are mainly formed between Ag and Cl atoms of the bis-carbene with –O–, –N–, and –C– of amino acids Asn 128, Asn 130, Lys 54, and Asn 129. Similarly, **bis-Ag-Si** forms 9 van der Waals interactions and 4 hydrogen bonds, of which, the metal compound AgCl and N-heterocyclic ring of silylene ligand create key interactions with –C–, –N–, and –O– of amino acids Asn 130, Gly 55, Asn 129, and Lys 54 (RMSD = 1.93 Å). The bis-germylene adduct **bis-Ag-Ge** performs 10 van der Waals interactions and 3 hydrogen bonds with amino acids Gly 55, Asn 130, and Asn 129. Although the number of interactions of **bis-Ag-Ge** with protein 4G9M is smaller than that of lighter homologues, its marked DS value of − 12.5 kcal mol^{-1} still indicates significant inhibitory effects derived from AgCl groups of the complexes. The elaborate inhibitory performance observed can be explained that **bis-Ag-E** complexes are more flexible due to their intramolecular groups of –C–, –N–, and –O–, and aromatic nitrogen atoms. Especially, the compounds contain N-heterocyclic rings, which perform strong affinity with amino acids of protein 4G9M. Regarding the referenced pesticide, although there are only 8 van der Waals interactions observed when docking validamycin onto protein 4G9M, the drug can form 6 hydrogen bonds with amino acids Asp 105, Arg 107, Lys 54, and Arg 107. Notably, the –O– groups of the pesticide interact strongly with –C–, –N–, and –O– of amino acids through H–donors and H–receptors. In brief, the inhibitability towards protein 4G9M of the complexes and validamycin can be assessed in the following order: **bis-Ag-C** > **bis-Ag-Si** > **bis-Ag-Ge** > validamycin > **Ag-C** ≈ **Ag-Si** ≈ **Ag-Ge**.

Docking results in Tables 3 and 4 show the DS values of silver-tetrylene (**Ag-C**, **Ag-Si, Ag-Ge**) if they inhibit protein 6JBR of *M. oryzae*. The values vary between − 12.9 and − 13.4 kcal mol^{-1}. The corresponding figures for **bis-Ag-C**, **bis-Ag-Si**, and **bis-Ag-Ge** are − 16.3 kcal mol^{-1}, − 18.1 kcal mol^{-1}, and − 18.4 kcal mol^{-1}, respectively. The differential between the figures is insignificant, while tricyclazole inhibits into the protein 6JBR with the lowest DS value, standing at just − 10.7 kcal·mol^{-1}. Silver-carbene adduct **Ag-C** forms 15 van der Waals interactions and 3 hydrogen bonds. In detail, its N-heterocyclic ring and phenyl ring create interactions with –C–, –N–, and –NH– of amino

Table 4 Molecular docking simulation results with critical interactions between the complexes and 6JBR amino acids: interaction distance between amino acids, site–site binding, energy, cation–π, π–π bonds, ionic interactions, and total hydrogen bonds

Complex (ligand–protein)	Ligand	Protein		Interactions	Distance (Å)	E (kcal·mol^{-1})	Hydrogen bonds
Ag-C-6JBR	6-ring	C	Gly 42	π–H	3.61	− 0.6	3
	5-ring	N	Gly 43	π–H	3.91	− 3.4	
	5-ring	NH	Arg 289	π–cation	3.67	− 5.7	
Ag-Si-6JBR	Ag	O	Asp 153	Metal	2.86	− 4.0	4
	Si	O	Asp 153	Ionic	3.98	− 0.5	
	6-ring	C	Gly 42	π–H	3.86	− 0.7	
	5-ring	N	Leu 44	π–H	3.97	− 1.0	
Ag-Ge-6JBR	Ge	N	Gly 43	H–acceptor	3.34	− 0.3	4
	Ge	NH	Arg 289	H–acceptor	3.55	−2.5	
	6-ring	C	Gly 42	π–H	3.81	− 1.0	
	5-ring	N	Gly 43	π–H	3.99	− 0.6	
bis-Ag-C-6JBR	Cl	N	Gly 42	H–acceptor	2.89	− 3.5	7
	Cl	C	Leu 392	H–acceptor	3.96	− 1.6	
	Ag	O	Thr 46	Metal	2.82	− 1.4	
	Ag	O	Glu 396	Ionic	3.55	− 1.7	
	5-ring	N	Gly 43	π–H	3.56	− 1.2	
	6-ring	N	Lys 257	π–cation	3.49	− 1.3	
	5-ring	N	Arg 289	π–cation	3.46	− 0.6	
bis-Ag-Si-6JBR	Cl	C	Leu 392	H–acceptor	3.84	− 1.7	10
	Cl	C	Gly 42	H–acceptor	2.93	− 0.9	
	Si	N	Arg 289	H–acceptor	3.21	− 1.5	
	Si	NH	Arg 289	H–acceptor	3.6	− 0.4	
	Ag	O	Thr 46	Metal	2.95	− 0.8	
	Si	O	Glu 396	Ionic	3.04	− 4.2	
	Si	O	Glu 396	Ionic	3.54	− 1.7	
	5-ring	N	Gly 43	π–H	3.85	− 1.7	
	6-ring	N	Lys 257	π–cation	3.52	− 1.1	
	5-ring	NH	Arg 289	π–cation	3.66	− 4.0	
bis-Ag-Ge-6JBR	Cl	C	Gly 42	H–acceptor	2.93	− 1.0	11
	Cl	N	Leu 392	H–acceptor	4.26	− 0.7	
	Cl	C	Leu 392	H–acceptor	3.8	− 1.7	
	Ge	N	Arg 289	H–acceptor	3.22	− 2.4	
	Ge	NH	Arg 289	H–acceptor	3.56	− 0.4	
	Ag	O	Thr 46	Metal	3	− 1.1	
	Ge	O	Glu 396	Ionic	3.14	− 3.6	
	Ge	O	Glu 396	Ionic	3.36	− 2.5	
	5-ring	N	Gly 43	π–H	3.9	− 1.4	
	6-ring	N	Lys 257	π–cation	3.64	− 0.6	
	5-ring	NH	Arg 289	π–cation	3.68	− 2.8	
Tricyclazole-6JBR	S	O	Asp 153	H–donor	3.45	− 2.3	4
	N	N	Asn 21	H–acceptor	3.61	− 2.7	
	N	N	Asn 21	H–acceptor	3.8	− 0.7	
	N	NH	Arg 22	H–acceptor	3.47	− 1.6	

acids Gly 42, Gly 43, and Arg 289 (RMSD = 1.52 Å). Silver-silylene **Ag-Si** and silver-germylene **Ag-Ge** respectively create 14 and 16 van der Waals interactions with amino acids of protein 6JBR and each 4 hydrogen bonds. The former has interactions mainly on Ag, Si, phenyl rings, and N-heterocyclic rings with –C–, –N–, and –NH– of amino acids Asp 153, Gly 42, and Leu 44 (RMSD = 1.30 Å) while the latter has germanium center atom, phenyl ring, and N-heterocyclic ring interactions with amino acids Gly 43, Arg 289, and Gly 42 through –C–, –N–, and –NH– groups

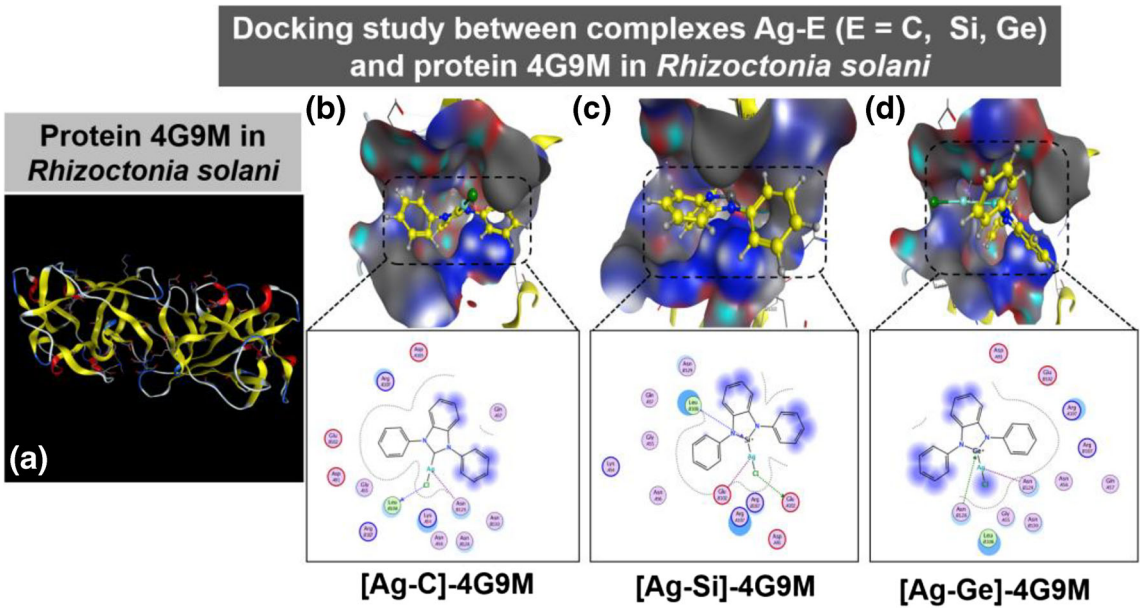

Fig. 7 Protein 4G9M docked with silver-tetrylene complexes: **Ag-C**, **Ag-Si**, **Ag-Ge**. **a** Crystal structure of protein 4G9M in *Rhizoctonia solani*. Docking simulation of the interaction between **Ag-C**, **Ag-Si**, **Ag-Ge,** and protein 4G9M. **b [Ag-C]-4G9M**. **c [Ag-Si]-4G9M. d [Ag-Ge]-4G9M**

(RMSD = 1.56 Å). Tables 3 and 4 also reveal considerable differences between the bis-silver-tetrylene complexes if they are allowed to inhibit the protein 6JBR. These include 20 van der Waals interactions for **bis-Ag-C** and 21 van der Waals interactions for **bis-Ag-Si** and **bis-Ag-Ge**. In fact, the **bis-Ag-C** complex exhibits strong interaction between AgCl, phenyl ring, N-heterocyclic ring of bis-carbene ligand, and protein 6JBR. This is formed by 7 different types of interactions, including cation–π, π–H bonds, ionic interactions, and H–acceptor between –O–, –N–, and –C– of amino acids Gly 42, Leu 392, Thr 46, Glam 396, Gly 43, and Lys 257, Arg 289 with RMSD = 1.69 Å. However, the heavier homologues **bis-Ag-Si** and **bis-Ag-Ge** could inhibit protein 6JBR even more strongly, based on (i) 10 different types of interaction for **[bis-Ag-Si]-6JBR**, of which, the main interactions include H–acceptor, cation–π, π–H bonds, ionic interactions of amino acids Leu 392, Gly 42, Arg 289, Thr 46, Glam 396, Gly 43, Lys 257, Arg 289 and AgCl, Si central atoms as well as phenyl ring, N-heterocyclic ring for **bis-Ag-Si**; (ii) 11 types of interaction for **[bis-Ag-Ge]-6JBR**, of which the significant

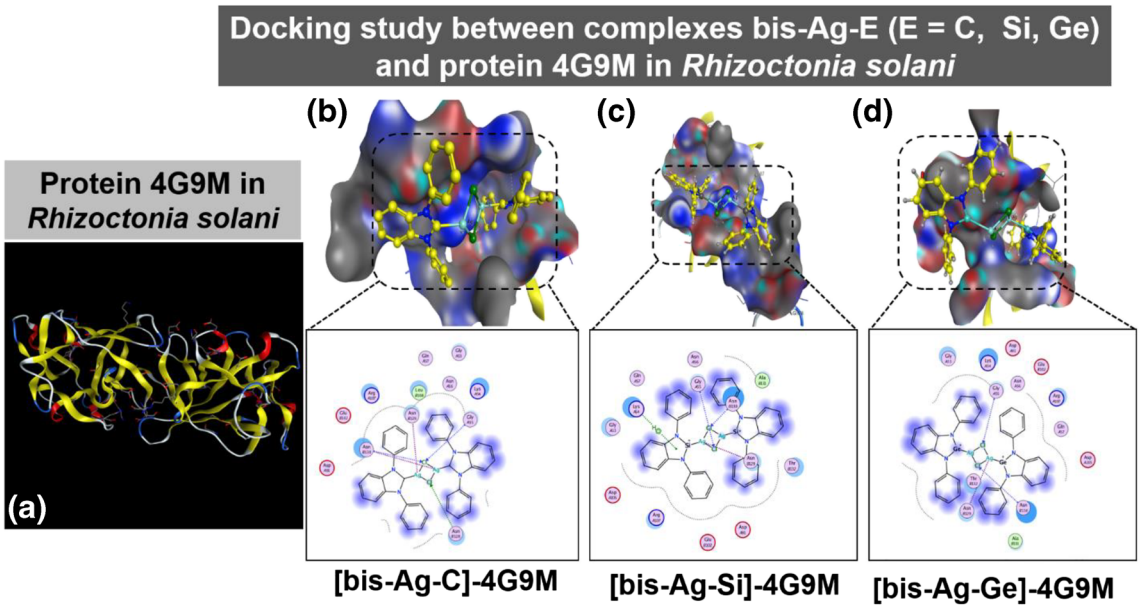

Fig. 8 Protein 4G9M docked with silver-tetrylene complexes: **bis-Ag-C**, **bis-Ag-Si**, **bis-Ag-Ge**. **a** Crystal structure of protein 4G9M in *Rhizoctonia solani*. Docking simulation of the interaction between **bis-Ag-C**, **bis-Ag-Si**, **bis-Ag-Ge**, and protein 4G9M. **b [bis-Ag-C]-4G9M. c [bis-Ag-Si]-4G9M. d [bis-Ag-Ge]-4G9M**

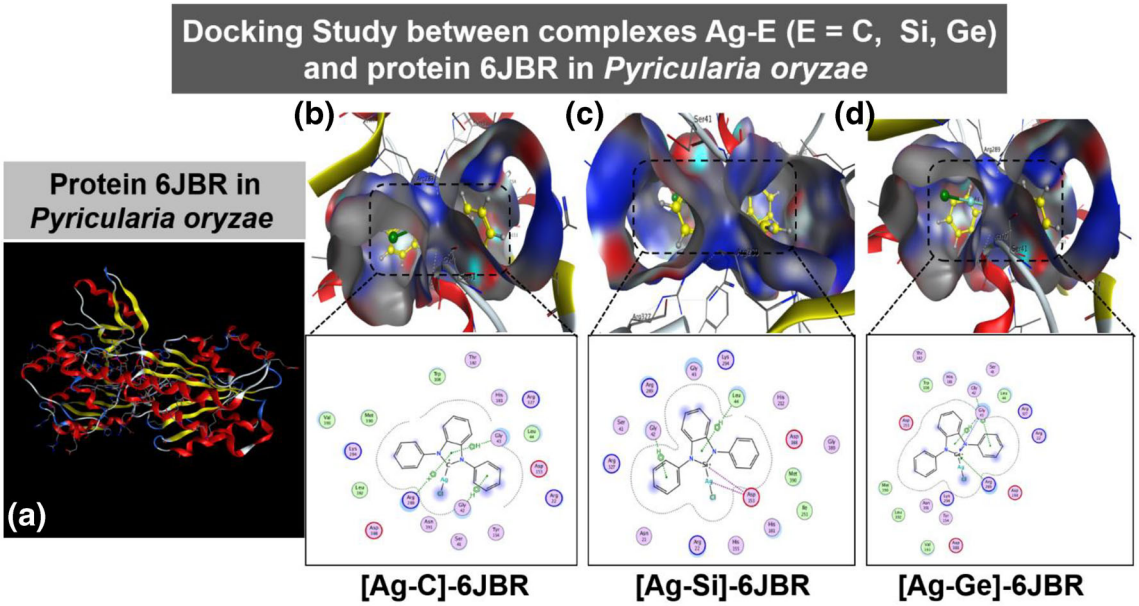

Fig. 9 Protein 6JBR docked with silver-tetrylene complexes: **Ag-C**, **Ag-Si**, **Ag-Ge**. **a** Crystal structure of protein 6JBR in *Magnaporthe oryzae*. Docking simulation of the interaction between **Ag-C**, **Ag-Si**, **Ag-Ge**, and protein 6JBR. **b [Ag-C]-6JBR. c [Ag-Si]-6JBR**. **d [Ag-Ge]-6JBR**

interactions include H–acceptor, π–H bonds, ionic interactions of amino acids Gly 42, Leu 392, Arg 289, Thr 46, Glam 396, Gly 43, Lys 257, Arg 289 and AgCl, Ge central atoms N-heterocyclic ring for **bis-Ag-Ge** adduct. These interactions are strong-binding hydrogen bonds listed in detail in Table 4. Regarding the referenced pesticide, tricyclazole creates 9 van der Waals interactions and 4 hydrogen bonds via interactions of –S– and –N– in the drug structure and –O–, –N–, and –NH– of amino acids Asp 153, Asn 21, and Arg 22. Docking results also reveal that the inhibitability towards protein 6JBR of silver-tetrylene complexes **Ag-E** is weaker than that of tricyclazole. Meanwhile, the bis-silver-tetrylene complexes **bis-Ag-E** perform better inhibitability than both categories. In brief, the inhibitory effects on protein 6JBR of the complexes and tricyclazole can be assessed by the following order: **bis-Ag-C** > **bis-Ag-Si** ≈ **bis-Ag-Ge** > tricyclazole ≈ **Ag-C** ≈ **Ag-Si** ≈ **Ag-Ge**. This can be explained by the contribution of numerous N-heterocyclic and phenyl rings in the versatile tetrylene ligands as well as of metal compounds AgCl with the presence of ion Ag^+.

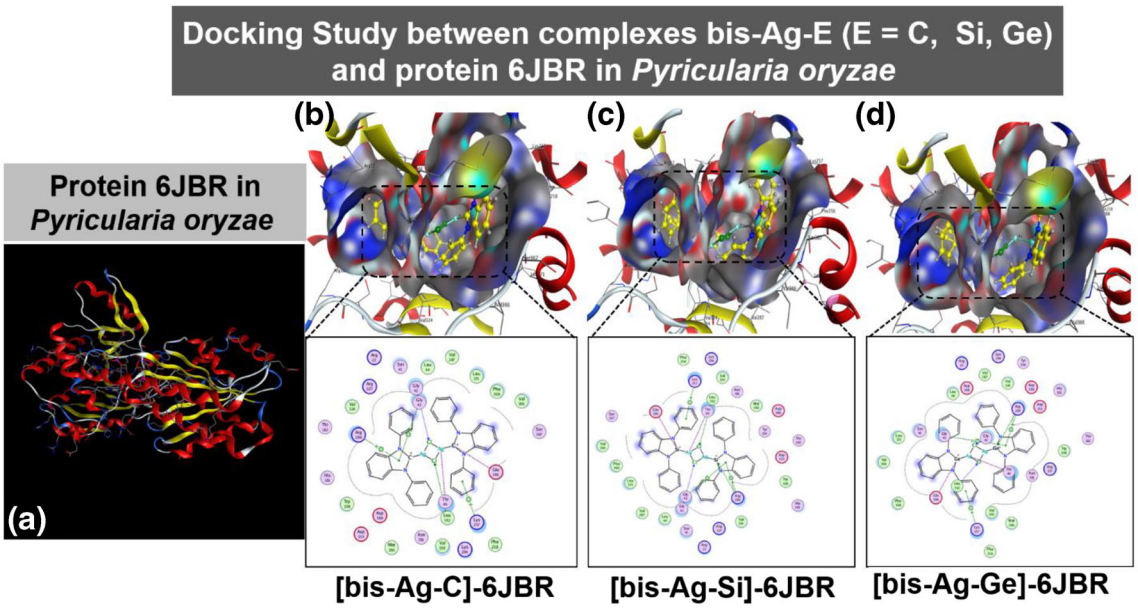

Fig. 10 Protein 6JBR docked with silver-tetrylene complexes: **bis-Ag-C**, **bis-Ag-Si**, **bis-Ag-Ge**. **a** Crystal structure of protein 6JBR in *Magnaporthe oryzae*. Docking simulation of the interaction between **bis-Ag-C**, **bis-Ag-Si**, **bis-Ag-Ge**, and protein 6JBR. **b [bis-Ag-C]-6JBR. c [bis-Ag-Si]-6JBR. d [bis-Ag-Ge]-6JBR**

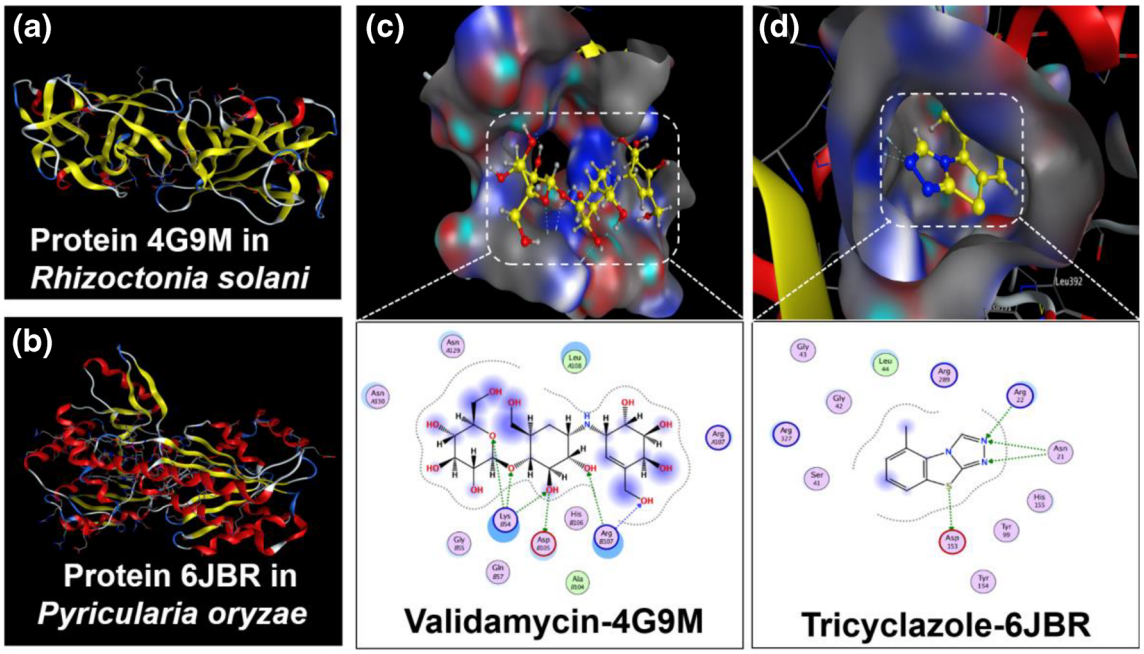

Fig. 11 2D and 3D docking simulation of protein 4G9M docked with validamycin and protein 6JBR docked with tricyclazole. **a** Crystal structure of protein 4G9M in *Rhizoctonia solani*. **b** Crystal structure of protein 6JBR in *Magnaporthe oryzae*. Docking simulation of the interaction between validamycin and protein 4G9M, tricyclazole, and protein 6JBR. **c** Validamycin-4G9M. **d** Tricyclazole-6JBR

Results obtained from the molecular docking models show that bis-silver-tetrylene complexes **bis-Ag-E** have strong inhibitory effects onto both 4G9M protein of *R. solani* and protein 6JBR of *M. oryzae*.

Conclusions

The present study demonstrates a promising approach to the use of the versatile tetrylene complexes to inhibit the attacks of fungi *R. solani* causing sheath blight in rice and fungi *M. oryzae* causing blast rice disease. Docking simulation results indicate that the selected tetrylene complexes are active for inhibiting the proteins 4G9M and 6JBR of *R. solani* and *M. oryzae*, respectively. Bis-silver-tetrylene complexes (**bis-Ag-C, bis-Ag-Si, bis-Ag-Ge**) exhibit the strongest inhibitory effects on both proteins 4G9M and 6JBR. The respective orders of their inhibitability towards proteins 4G9M and 6JBR are as follows: **bis-Ag-C** > **bis-Ag-Si** > **bis-Ag-Ge** > validamycin > **Ag-C** ≈ **Ag-Si** ≈ **Ag-Ge**; and **bis-Ag-C** > **bis-Ag-Si** ≈ **bis-Ag-Ge** > tricyclazole≈ **Ag-C** ≈ **Ag-Si** ≈ **Ag-Ge**. The docking score energies of potential tetrylene complexes for protein 4G9M in *R. solani* fungi are from − 13.7 to − 9.6 kcal mol^{-1}. The corresponding figures for protein 6JBR in *M. oryzae* are from − 18.4 to − 12.9 kcal·mol^{-1}. The root-mean-square deviation values are lower than 2 Å in any system. The structures of the potential tetrylene complexes exhibit the good site–site binding with the protein 4G9M and protein 6JBR based on the hydrogen bond interactions, cation–π, π–π bonds, and ionic interactions, interaction distance between amino acids and ligands, and van der Waals interactions between the studied complexes and essential amino acids of the two proteins. Significantly, the results also reveal that the inhibitory capacity of potential tetrylene complexes on the two proteins is based on the correlation between the average of docking score energy, site–site active interactions of potential tetrylene complexes-proteins, polarizability, and size of the potential complexes. Predictive results by molecular docking simulation in this study primarily confirm that the six complexes (**Ag-E** and **bis-Ag-E** with **E** = C, Si, Ge) are potential complexes and act as a reference source of data for further research on the development of new agents to inhibit proteins 4G9M and 6JBR in particular and to prevent fungi *R. solani* and fungi *M. oryzae* affecting rice plants in general. This opens an environmentally advanced and molecularly effective alternative for current pesticide products, especially validamycin and tricyclazole.

Funding This research is funded by the Vietnam National Foundation for Science and Technology Development (NAFOSTED) under grant number 104.06-2017.303.

Compliance with ethical standards

Conflict of interest The authors declare that they have no conflict of interest.

References

1. Pham DC, Nguyen TH, Ngoc UTP, Le NTT, Tran TV, Nguyen DH (2018) Preparation, characterization and antifungal properties of chitosan-silver nanoparticles synergize fungicide against Pyricularia oryzae. J Nanosci Nanotechnol 18(8):5299–5305
2. Banniza S, Holderness M (2001) Rice sheath blight—pathogen biology and diversity. Major fungal diseases of rice. Springer, pp 201–211
3. Richa K, Tiwari IM, Kumari M, Devanna B, Sonah H, Kumari A, Nagar R, Sharma V, Botella JR, Sharma TR (2016) Functional characterization of novel chitinase genes present in the sheath blight resistance QTL: qSBR11-1 in rice line tetep. Front Plant Sci 7:244
4. Hahn M (2014) The rising threat of fungicide resistance in plant pathogenic fungi: Botrytis as a case study. J Chem Biol 7(4):133–141
5. Belden J, McMurry S, Smith L, Reilley P (2010) Acute toxicity of fungicide formulations to amphibians at environmentally relevant concentrations. Environ Toxicol Chem 29(11):2477–2480
6. Tomšič B, Simončič B, Orel B, Žerjav M, Schroers H, Simončič A, Samardžija Z (2009) Antimicrobial activity of AgCl embedded in a silica matrix on cotton fabric. Carbohydr Polym 75(4):618–626
7. Vertelov G, Krutyakov YA, Efremenkova O, Olenin AY, Lisichkin G (2008) A versatile synthesis of highly bactericidal Myramistin® stabilized silver nanoparticles. Nanotechnology 19(35):355707
8. Zhang Y, Peng H, Huang W, Zhou Y, Yan D (2008) Facile preparation and characterization of highly antimicrobial colloid Ag or Au nanoparticles. J Colloid Interface Sci 325(2):371–376
9. Kim K-J, Sung WS, Suh BK, Moon S-K, Choi J-S, Kim JG, Lee DG (2009) Antifungal activity and mode of action of silver nanoparticles on Candida albicans. Biometals 22(2):235–242
10. Kim YS, Kim JS, Cho HS, Rha DS, Kim JM, Park JD, Choi BS, Lim R, Chang HK, Chung YH (2008) Twenty-eight-day oral toxicity, genotoxicity, and gender-related tissue distribution of silver nanoparticles in Sprague-Dawley rats. Inhal Toxicol 20(6):575–583
11. Kim J, Lee J, Kwon S, Jeong S (2009) Preparation of biodegradable polymer/silver nanoparticles composite and its antibacterial efficacy. J Nanosci Nanotechnol 9(2):1098–1102
12. Peterson LG (1990) Tricyclazole for control of Pyricularia oryzae on rice: the relationship of the mode of action and disease occurrence and development. Pest Management in Rice. Springer, pp 122–130
13. Woloshuk C, Sisler H, Vigil E (1983) Action of the antipenetrant, tricyclazole, on appressoria of Pyricularia oryzae. Physiol Plant Pathol 22(2):245–IN21
14. Woloshuk CP, Sisler HD, Tokousbalides MC, Dutky SR (1980) Melanin biosynthesis in Pyricularia oryzae: site of tricyclazole inhibition and pathogenicity of melanin-deficient mutants. Pestic Biochem Physiol 14(3):256–264
15. Wasimfiroz M, Hosagoudar G, Narayanaswamy H (2018) Management of leaf blast and neck blast of rice caused by Pyricularia oryzae under field condition. J Pharmacogn. Phytochem 7(2):968–971
16. Kulmitra AK, Kumar VS, Thejesha A, Ghosh A, Sahu P (2017) In vitro evaluation of fungicides against Pyricularia oryzae (Cav.) causing rice blast disease. IJCS 5(4):506–509
17. (2017) COMMISSION REGULATION (EU) 2017/983 Amending Annexes III and V to Regulation (EC) No 396/2005 of the European Parliament and of the Council as regards maximum residue levels for tricyclazole in or on certain products. Official Journal of the European Union
18. Li J, Duan Y, Bian C, Pan X, Yao C, Wang J, Zhou M (2019) Effects of validamycin in controlling Fusarium head blight caused by Fusarium graminearum: inhibition of DON biosynthesis and induction of host resistance. Pestic Biochem Physiol 153:152–160
19. Singh R, Singh B, Singh A, Singh UP, Kureel R (2010) Management of sheath blight in rice through application of validamycin, Trichoderma harzianum and Pseudomonas fluorescence. J Nat Appl Sci 2(1):121–125
20. Pralhad SP (2020) Evaluation of actinobacteria for biocontrol of sheath blight in rice. J Pharmacogn Phytochem 9(3):371–376
21. Wu Q, Zhang L, Xia H, Yu C, Dou K, Li Y, Chen J (2017) Omics for understanding synergistic action of validamycin A and Trichoderma asperellum GDFS1009 against maize sheath blight pathogen. Sci Rep 7(1):1–11
22. Lamsal K, Kim SW, Jung JH, Kim YS, Kim KS, Lee YS (2011) Application of silver nanoparticles for the control of Colletotrichum species in vitro and pepper anthracnose disease in field. Mycobiology 39(3):194–199
23. Mishra S, Singh H (2015) Biosynthesized silver nanoparticles as a nanoweapon against phytopathogens: exploring their scope and potential in agriculture. Appl Microbiol Biotechnol 99(3):1097–1107
24. Azam A, Ahmed AS, Oves M, Khan M, Memic A (2012) Size-dependent antimicrobial properties of CuO nanoparticles against Gram-positive and-negative bacterial strains. Int J Nanomedicine 7:3527
25. Applerot G, Lellouche J, Lipovsky A, Nitzan Y, Lubart R, Gedanken A, Banin E (2012) Understanding the antibacterial mechanism of CuO nanoparticles: revealing the route of induced oxidative stress. Small 8(21):3326–3337
26. Kim JS, Kuk E, Yu KN, Kim J-H, Park SJ, Lee HJ, Kim SH, Park YK, Park YH, Hwang C-Y (2007) Antimicrobial effects of silver nanoparticles. Nanomed Nanotechnol Biol Med 3(1):95–101
27. Raffi M, Mehrwan S, Bhatti TM, Akhter JI, Hameed A, Yawar W, ul Hasan MM (2010) Investigations into the antibacterial behavior of copper nanoparticles against Escherichia coli. Ann Microbiol 60(1):75–80
28. Kascatan-Nebioglu A, Panzner MJ, Tessier CA, Cannon CL, Youngs WJ (2007) N-Heterocyclic carbene–silver complexes: a new class of antibiotics. Coord Chem Rev 251(5–6):884–895
29. Dyker CA, Lavallo V, Donnadieu B, Bertrand G (2008) Synthesis of an extremely bent acyclic allene (a "carbodicarbene"): a strong donor ligand. Angew Chem Int Ed 47(17):3206–3209
30. Fürstner A, Alcarazo M, Goddard R, Lehmann CW (2008) Coordination chemistry of Ene-1, 1-diamines and a prototype "carbodicarbene". Angew Chem Int Ed 47(17):3210–3214
31. Banti CN, Hadjikakou SK (2013) Anti-proliferative and anti-tumor activity of silver (I) compounds. Metallomics 5(6):569–596
32. Eloy L, Jarrousse AS, Teyssot ML, Gautier A, Morel L, Jolivalt C, Cresteil T, Roland S (2012) Anticancer activity of silver–N-heterocyclic carbene complexes: caspase-independent induction of apoptosis via mitochondrial apoptosis-inducing factor (AIF). ChemMedChem 7(5):805–814
33. Guin J, De Sarkar S, Grimme S, Studer A (2008) Biomimetic carbene-catalyzed oxidations of aldehydes using TEMPO. Angew Chem Int Ed 47(45):8727–8730
34. Skamnaki VT, Kantsadi AL, Leonidas DD (2013) Crystal structure of the Rhizoctonia solani agglutinin. https://www.rcsb.org/structure/4G9M.
35. Wang S, Zhao Y, Wang D, Liu J (2019) Tps1/UDP/T6P complex. https://www.rcsb.org/structure/6JBR.
36. Frenking G, Tonner R (2011) Carbodicarbenes—divalent carbon (0) compounds exhibiting carbon–carbon donor–acceptor bonds. Wiley Interdiscip Rev Comput Mol Sci 1(6):869–878
37. Labute P (2000) A widely applicable set of descriptors. J Mol Graph Model 18(4–5):464–477
38. Boehme C, Frenking G (1998) N-Heterocyclic carbene, silylene, and germylene complexes of MCl (M = Cu, Ag, Au). A theoretical study1. Organometallics 17(26):5801–5809
39. Frisch MJ, Trucks GW, Schlegel HB, Scuseria GE, Robb MA, Cheeseman JR, Scalmani G, Barone V, Petersson GA, Nakatsuji

H, Li X, Caricato M, Marenich A, Bloino J, Janesko BG, Gomperts R, Mennucci B, Hratchian HP, Ortiz JV, Izmaylov AF, Sonnenberg JL, Williams-Young D, Ding F, Lipparini F, Egidi F, Goings J, Peng B, Petrone A, Henderson T, Ranasinghe D, Zakrzewski VG, Gao J, Rega N, Zheng G, Liang W, Hada M, Ehara M, Toyota K, Fukuda R, Hasegawa J, Ishida M, Nakajima T, Honda T, Kitao O, Nakai H, Vreven T, Throssell K, Montgomery JA, Peralta Jr JE, Ogliaro F, Bearpark M, Heyd JJ, Brothers E, Kudin KN, Staroverov VN, Keith T, Kobayashi R, Normand J, Raghavachari K, Rendell A, Burant JC, Iyengar SS, Tomasi J, Cossi M, Millam JM, Klene M, Adamo C, Cammi R, Ochterski JW, Martin RL, Morokuma K, Farkas O, Foresman JB, Fox DJ (2016) Gaussian 09. Revision A.02. Gaussian, Inc., Wallingford

40. Gasteiger J, Marsili M (1980) Iterative partial equalization of orbital electronegativity—a rapid access to atomic charges. Tetrahedron 36(22):3219–3228